

Article

# Artifact-Free Microstructures in the Interfacial Reaction between Eutectic In-48Sn and Cu Using Ion Milling

Fu-Ling Chang, Yu-Hsin Lin, Han-Tang Hung, Chen-Wei Kao and C. R. Kao \* 

Department of Materials Science and Engineering, National Taiwan University, Taipei 106216, Taiwan

\* Correspondence: crkao@ntu.edu.tw

**Abstract:** Eutectic In-48Sn was considered a promising candidate for low-temperature solder due to its low melting point and excellent mechanical properties. Both  $\text{Cu}_2(\text{In},\text{Sn})$  and  $\text{Cu}(\text{In},\text{Sn})_2$  formation were observed at the In-48Sn/Cu interface after 160 °C soldering. However, traditional mechanical polishing produces many defects at the In-48Sn/Cu interface, which may affect the accuracy of interfacial reaction investigations. In this study, cryogenic broad  $\text{Ar}^+$  beam ion milling was used to investigate the interfacial reaction between In-48Sn and Cu during soldering. The phase  $\text{Cu}_6(\text{Sn},\text{In})_5$  was confirmed as the only intermetallic compound formed during 150 °C soldering, while  $\text{Cu}(\text{In},\text{Sn})_2$  formation was proven to be caused by room-temperature aging after soldering. Both the  $\text{Cu}_6(\text{Sn},\text{In})_5$  and  $\text{Cu}(\text{In},\text{Sn})_2$  phases were confirmed by EPMA quantitative analysis and TEM selected area electron diffraction. The microstructure evolution and growth mechanism of  $\text{Cu}_6(\text{Sn},\text{In})_5$  during soldering were proposed. In addition, the Young's modulus and hardness of  $\text{Cu}_6(\text{Sn},\text{In})_5$  were determined to be  $119.04 \pm 3.94$  GPa and  $6.28 \pm 0.13$  GPa, respectively, suggesting that the doping of In in  $\text{Cu}_6(\text{Sn},\text{In})_5$  has almost no effect on Young's modulus and hardness.

**Keywords:** low-temperature soldering; interconnection; Cu-In-Sn intermetallic compounds; interfacial reaction; mechanical properties



**Citation:** Chang, F.-L.; Lin, Y.-H.; Hung, H.-T.; Kao, C.-W.; Kao, C.R. Artifact-Free Microstructures in the Interfacial Reaction between Eutectic In-48Sn and Cu Using Ion Milling. *Materials* **2023**, *16*, 3290. <https://doi.org/10.3390/ma16093290>

Academic Editors: Sergei A. Kulinich, Aleksandr Kuchmizhak, Mitsuhiro Honda and Valery A. Svetlichnyy

Received: 30 March 2023

Revised: 17 April 2023

Accepted: 20 April 2023

Published: 22 April 2023



**Copyright:** © 2023 by the authors. Licensee MDPI, Basel, Switzerland. This article is an open access article distributed under the terms and conditions of the Creative Commons Attribution (CC BY) license (<https://creativecommons.org/licenses/by/4.0/>).

## 1. Introduction

Due to the toxicity of Pb, there has been increasing demand for the use of Pb-free solders since the beginning of the 21st century. Currently, lead-free Sn-based solder alloys are widely used in electronic packaging systems [1,2]. Although using Sn as a soldering material avoids Pb toxicity, it results in an increase in soldering temperature, as the melting point of most Sn-based solders is approximately 200 °C. Temperature-sensitive chips are unable to withstand this high-temperature bonding, so low-temperature soldering materials need to be developed. A reduction in soldering temperature could also decrease the energy used in the soldering process, which would be environmentally beneficial.

Eutectic alloys are ideal because of their low soldering temperatures, making them easy to apply in industrial production. Therefore, Sn-based binary alloys doped with Ga, Zn, Bi, and In have been recognized as potential candidates for low-temperature bonding [1–3]. However, these alloying elements have drawbacks; for instance, using an alloy containing Ga is impractical due to its low melting point. The addition of Zn in the alloy results in poor wettability, reliability, and corrosion resistance, and the addition of Bi can cause brittle failure and segregation in the alloy. The eutectic In-48Sn alloy is a promising soldering material, as it is non-toxic and has a melting point of 120 °C. This alloy also has good wettability, excellent ductility, and a long fatigue life [4]. In addition, it was reported that various diameters of In-48Sn solder wires and rods can be produced easily because of the ductility and high elongation of In-48Sn [5]. For these reasons, eutectic In-48Sn alloy can be used in temperature-sensitive chips, such as biochips and flexible chips.

Solid–liquid interdiffusion (SLID) bonding is a well-developed and widely used technique in the electronic packaging industry. Generally, a SLID metal system consists

of two layers: a high-melting-point substrate layer and a low-melting-temperature solder layer. During the bonding process, the joint is heated to a temperature greater than the melting point of the solder layer. The molten solder reacts with the substrate layer to form at least one IMC and continues until the entire solder layer transforms into IMCs with much higher melting temperatures than the original solder. Compared with the other conventional techniques used in the electronic packing industry, the most important benefit of SLID bonding is that the joint can be bonded at low temperatures and used in high-temperature applications due to the formation of high-melting-temperature IMCs.

Several studies have investigated the interfacial reaction between In-48Sn solder and Cu substrate. Phase identification of the formed IMCs at the In-48Sn/Cu interface was performed; two IMCs,  $\text{Cu}_2(\text{In,Sn})$  and  $\text{Cu}(\text{In,Sn})_2$ , formed after reflowing at 160 °C [6]. The voids existing at the In-48Sn/Cu interface were proven to be Kirkendall voids formed during reflowing and the solid-state aging process [7,8]. The growth mechanism of  $\text{Cu}_2(\text{In,Sn})$  and  $\text{Cu}(\text{In,Sn})_2$  and the phase transformation between these two phases were investigated [9–15]. It was found that  $\text{Cu}(\text{In,Sn})_2$  transformed to  $\text{Cu}_2(\text{In,Sn})$  when aging above 60 °C, while  $\text{Cu}_2(\text{In,Sn})$  transformed to  $\text{Cu}(\text{In,Sn})_2$  when aging below 60 °C. The relationship between IMC thickness and aging time was also determined. In an investigation of Cu addition to In-48Sn solder, the observed Cu-rich IMC was reported to be  $\eta\text{-Cu}_6(\text{Sn,In})_5$  [16,17]. In the Cu/In-48Sn/Cu interfacial reaction, where the In-48Sn is completely consumed,  $\text{Cu}_6(\text{Sn,In})_5$  and  $\text{Cu}_3(\text{Sn,In})$  were observed at the interface after 250 °C bonding; only  $\text{Cu}_6(\text{Sn,In})_5$  was observed after 200 °C to 160 °C bonding [18–22]. The results of previous works imply that there is extremely fast formation of IMCs at the In-48Sn/Cu interface, which makes In-48Sn a promising SLID material [23]. However, the In-48Sn/Cu interface is easily destroyed during mechanical polishing, and the lack of an artifact-free In-48Sn/Cu interface may restrict the accurate analysis of microstructure evolution and phase identification at the interface.

In this study, the interfacial reaction between molten In-48Sn and Cu at 150 °C from tens of seconds to tens of minutes was studied. Cryogenic ion milling was used to produce an artifact-free interface so that the interface microstructure evolution, phase identification, and IMC growth mechanism could be investigated more accurately. Phase identification of each phase was confirmed by both chemical composition and crystallographic structure. Additionally, the IMC formed at the interface caused by room-temperature storage after soldering was also clarified.

## 2. Experimental Method

### 2.1. Sample Preparation

The eutectic In-48Sn solder was prepared by mixing and melting high-purity In (99.99%) and Sn shots (99.99%) under a vacuum. Oxygen-free Cu plates were cut to a size of 10 mm × 10 mm × 1 mm, ground using silicon carbide sandpaper, and polished with 3 µm and 1 µm polycrystalline diamond polishing fluid.

As shown in Figure 1, the amount of solder used was 0.15 (±0.001) g, and the circular reaction area had a diameter of 3 mm. The copper substrates were cleaned with sulfuric acid and isopropanol solutions. Halogen-free flux and Kapton tape with a temperature resistance exceeding 150 °C were used for sample preparation.

Once the In-48Sn solder was added, the sample was placed in a convection oven at 150 (±1) °C. After the liquid–solid reaction was complete, the sample was quenched in water.

### 2.2. Cross-Section Observation and Ion Milling

The alloy sample was metallographically polished prior to cross-sectional observation. However, during mechanical polishing, the silicon carbide particles on the sandpaper and diamond abrasives in the polishing fluid were embedded in the soft In-Sn alloy. It has been reported that ion milling can be used in place of mechanical polishing for samples that are damaged by mechanical polishing [24]. An ion milling system (Hitachi, IM4000Plus, Tokyo,

Japan) equipped with a liquid-nitrogen cryogenic system was used to prevent the In-48Sn solder in the sample from melting due to the heat generated during the ion milling process.

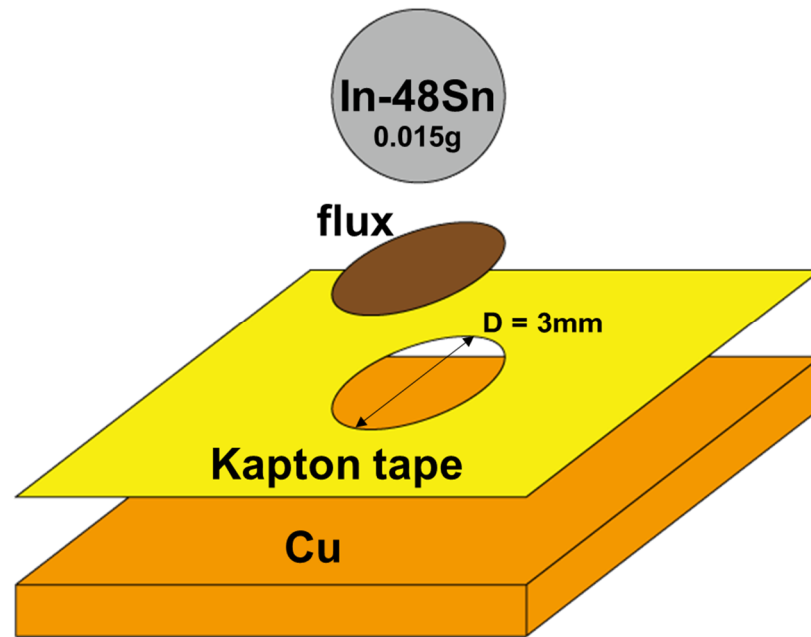


**Figure 1.** Schematic of the sample preparation.

The sample was ion milled at  $-50\text{ }^{\circ}\text{C}$  for 1.5 h to obtain an artifact-free cross-sectional micrograph of the solder/substrate interface, as shown in Figure 2. Scanning electron microscopy (SEM; Hitachi SU-5000, Tokyo, Japan) was used to observe the morphology and evolution of the solder/substrate interface. The chemical compositions of the solder and IMCs at the solder/substrate interface were analyzed using energy-dispersive X-ray spectroscopy (EDS; Bruker, Billerica, MA, USA) and an electron probe microanalyzer (EPMA; JEOL JXA-8530FPlus, Tokyo, Japan).

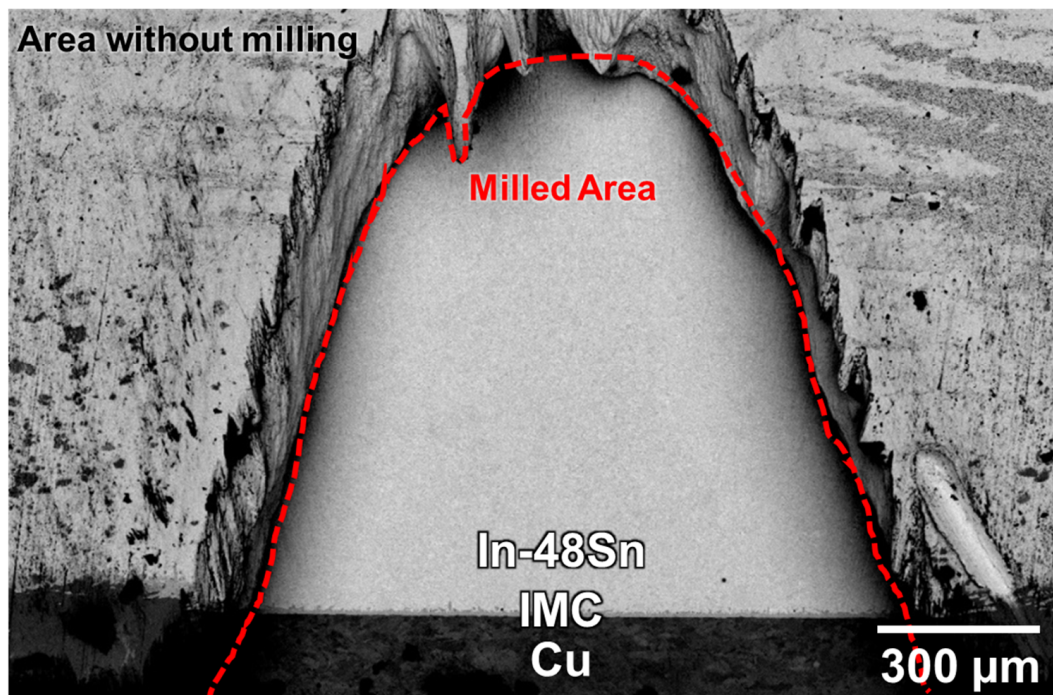


**Figure 2.** Cross-section micrograph showing the In-48Sn/Cu interface after ion milling.

### 2.3. Top-View Observation and Etching

The top-view morphology and crystallographic structures of the IMCs were observed using SEM and X-ray diffraction (XRD), respectively. The alloy sample was chemically etched to remove the excess solder and expose the IMCs. This allowed us to observe the top-view morphology and identify the crystallographic structures of the IMCs. A high-power X-ray diffractometer (18 kW) (Rigaku, TTRAX3, Tokyo, Japan) with a Cu-K $\alpha$  source was used to identify the crystallographic structures of the IMCs.

### 2.4. Mechanical Property Determination

Because the thickness of the IMCs was on the order of micrometers, nanoindentation testing (Hysitron TI 980 TriboIndenter with a Berkovich tip, Billerica, MA, USA) was used to analyze the mechanical properties of Cu<sub>6</sub>(Sn,In)<sub>5</sub> in this study.

## 3. Results and Discussion

### 3.1. Interfacial Microstructure

The In-48Sn/Cu sample was soldered at 150 °C for 80 min, followed by water quenching. The cross-section of the interface is shown in Figure 3a, and the top-view morphology of the IMCs after all the In-48Sn solder was removed by the etching solution is shown in Figure 3b. As shown in Figure 3, there are two distinct microstructure regions at the interface. The region in contact with the solder has a large quantity of rod-type IMCs, while the region in contact with the substrate is composed of a solder/IMC mixture. Similar observations have been reported in the solid–liquid reaction in Cu/In binary systems [24]. There are differences in the interface shape and phase of the IMCs between the In-48Sn/Cu and Cu/In systems. According to EDS quantitative analysis, the elemental composition of the IMC in both microstructures can be described as 56Cu-18In-26Sn (at.%), indicating that it is most likely to be Cu<sub>6</sub>(Sn,In)<sub>5</sub> rather than Cu<sub>2</sub>(In,Sn). This result will be confirmed using EPMA and XRD analysis, as discussed below.

### 3.2. Phase Identification

The EPMA elemental mapping and quantitative analysis are shown in Figure 4 and Table 1, respectively. The In-48Sn solder matrix was separated into  $\beta$  and  $\gamma$  phases, which is consistent with the reported In-Sn phase diagram [25]. As mentioned above, the elemental composition of the IMC in the mixed layer and the rod-type IMC is Cu<sub>6</sub>(Sn,In)<sub>5</sub>.

**Table 1.** EPMA quantitative analysis of  $\beta$ ,  $\gamma$ , and Cu<sub>6</sub>(Sn,In)<sub>5</sub>.

Phase	Cu (at.%)	In (at.%)	Sn (at.%)
$\beta$	0.8	71.9	27.3
$\gamma$	2.2	26.1	71.7
Rod-type Cu <sub>6</sub> (Sn,In) <sub>5</sub>	55.7	18.9	25.4
Cu <sub>6</sub> (Sn,In) <sub>5</sub> in the mixture layer	56.2	17.7	26.1

The compound Cu<sub>6</sub>Sn<sub>5</sub> is a common IMC in Sn-containing solder joints and is well known for its polymorphic transformation from  $\eta$ -Cu<sub>6</sub>Sn<sub>5</sub> (hexagonal, space group P63/mmc) to  $\eta'$ -Cu<sub>6</sub>Sn<sub>5</sub> (monoclinic, space group C2/c). This polymorphic transformation is accompanied by a volume change, which induces the formation and propagation of cracks and is considered an important factor leading to packaging failure.

XRD analysis was used to confirm the crystallographic structure of the IMC at the interface; the obtained diffraction pattern is shown in Figure 5. The remaining solder was completely etched; therefore, all of the peaks in the XRD pattern were from the IMCs and substrate. As shown in Figure 5, only Cu<sub>6</sub>(Sn,In)<sub>5</sub> and Cu peaks are present. This confirms that the chemical composition of both the rod-type IMCs and IMCs in the mixture layer is Cu<sub>6</sub>(Sn,In)<sub>5</sub>, which is consistent with the results of the EPMA quantitative analysis.

The appearance of several weak peaks in the XRD pattern can help distinguish whether the appearance of the IMC belongs to the  $\eta$ - $\text{Cu}_6\text{Sn}_5$  or  $\eta'$ - $\text{Cu}_6\text{Sn}_5$  phase. Weak peaks would indicate monoclinic  $\eta'$ - $\text{Cu}_6\text{Sn}_5$ , as it has relatively poor symmetry [12,23,24,26]. As shown in Figure 5, no monoclinic peaks can be observed from the XRD pattern, meaning that the  $\text{Cu}_6(\text{Sn},\text{In})_5$  at the interface is the high-temperature phase of  $\eta$ - $\text{Cu}_6\text{Sn}_5$ . This result is consistent with previous work, which found that the addition of In stabilized the high-temperature phase  $\eta$ - $\text{Cu}_6\text{Sn}_5$  at room temperature [26]. The results show that each diffraction peak from  $\text{Cu}_6(\text{Sn},\text{In})_5$  slightly deviates from In-free  $\eta$ - $\text{Cu}_6\text{Sn}_5$ . This is caused by a change in the interplanar spacing due to the replacement of Sn by In. The crystallographic structure information of Cu,  $\eta$ - $\text{Cu}_6\text{Sn}_5$ , and  $\eta'$ - $\text{Cu}_6\text{Sn}_5$  is from the Joint Committee on Powder Diffraction Standards (JCPDS) data file numbers 04-0836, 02-0713, and 45-1488.

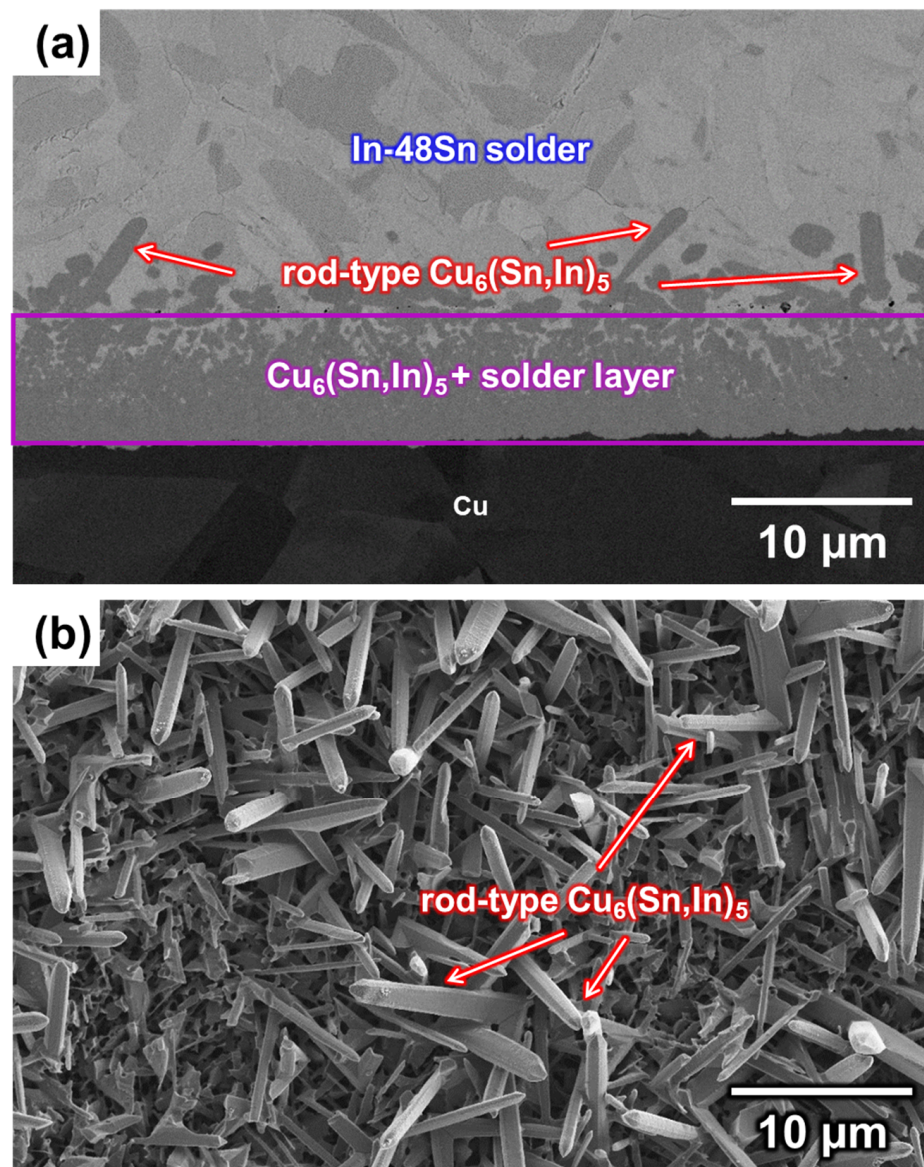


**Figure 3.** (a) Cross-section of the In-48Sn/Cu interface after soldering at 150 °C for 80 min and (b) top-view after removing all In-48Sn solder.

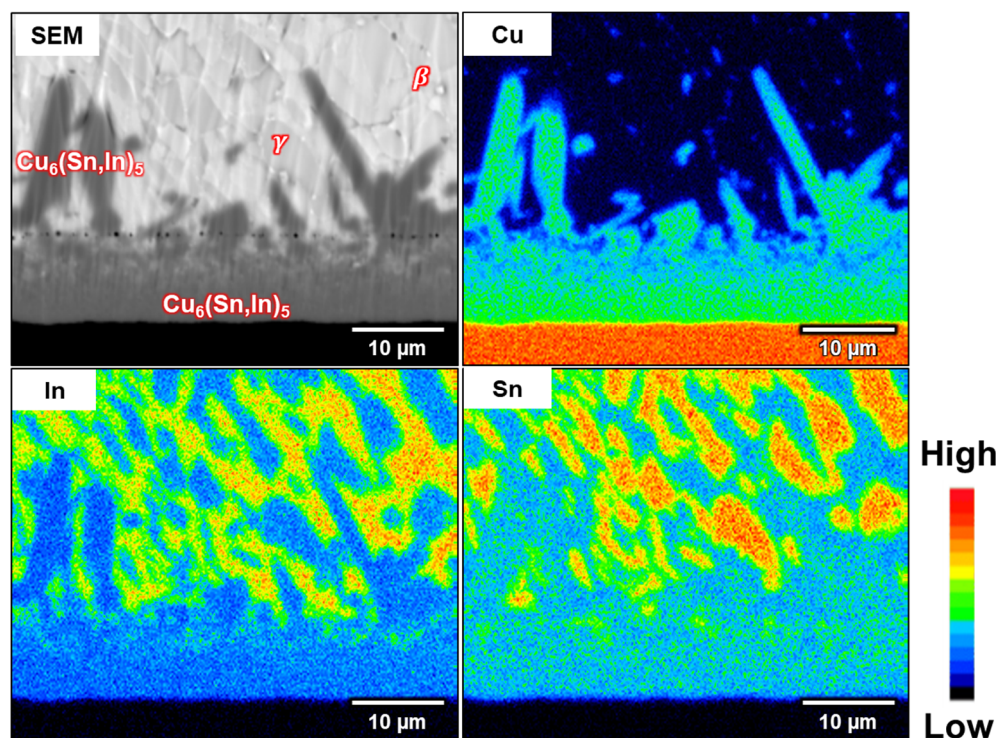


Figure 4. EPMA elemental mapping of the In-48Sn/Cu interface after soldering at 150 °C for 80 min.

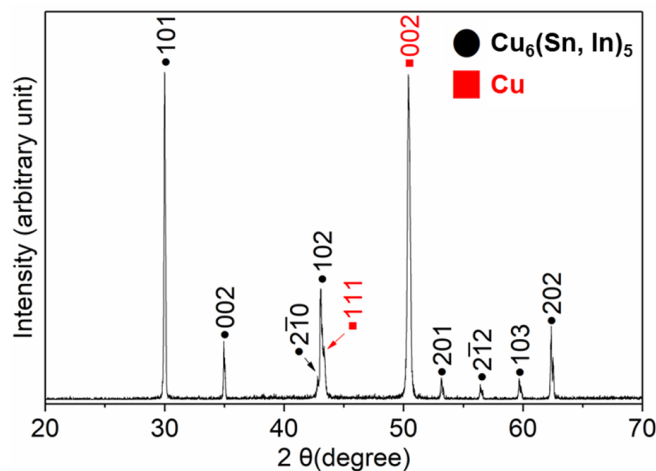
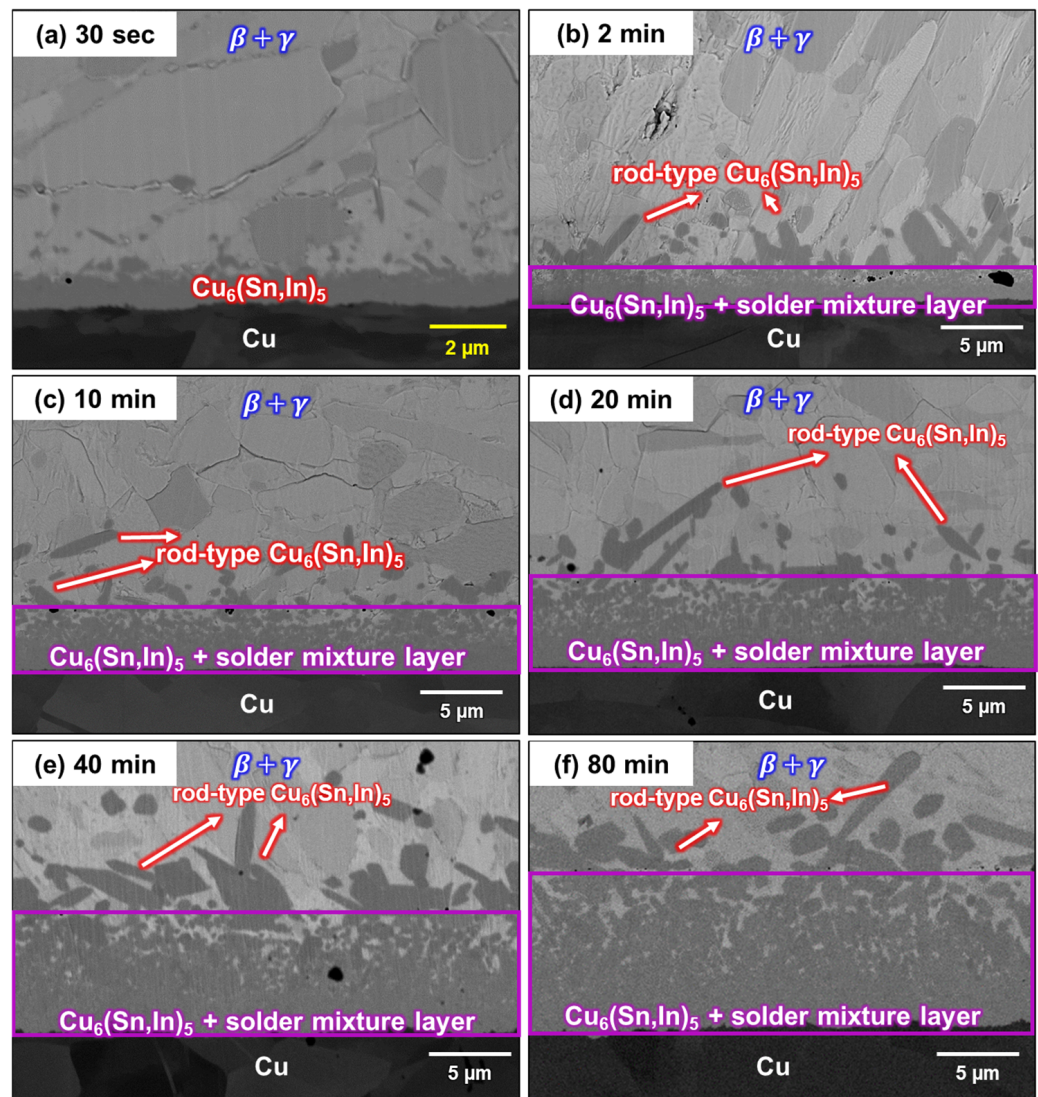


Figure 5. XRD pattern of  $\text{Cu}_6(\text{Sn},\text{In})_5$  and Cu substrate after soldering at 150 °C for 80 min.

### 3.3. Microstructure Evolution

As mentioned previously, there are two different microstructures at the interface: rod-type  $\text{Cu}_6(\text{Sn},\text{In})_5$  and a solder/ $\text{Cu}_6(\text{Sn},\text{In})_5$  mixture layer. The cross-section microstructure evolution of the liquid–solid reaction after soldering at 150 °C for 0.5 min, 2 min, 10 min, 20 min, 40 min, and 80 min is shown in Figure 6a–f. As shown in Figure 6, the thickness of the solder/ $\text{Cu}_6(\text{Sn},\text{In})_5$  layer formed during soldering increased with time. Furthermore, there is a non-uniform distribution in the solder/ $\text{Cu}_6(\text{Sn},\text{In})_5$  mixture layer, especially during long-term soldering. This non-uniformity can be described as  $\text{Cu}_6(\text{Sn},\text{In})_5$  dissolved in molten In-48Sn. While Sn and In diffuse downward to form  $\text{Cu}_6(\text{Sn},\text{In})_5$ , In-48Sn solder simultaneously dissolves  $\text{Cu}_6(\text{Sn},\text{In})_5$ . This can explain why the proportion of  $\text{Cu}_6(\text{Sn},\text{In})_5$  decreases as it moves toward the In-48Sn solder.



**Figure 6.** Micrographs of the In-48Sn/Cu interfaces after soldering at 150 °C for (a) 0.5 min, (b) 2 min, (c) 10 min, (d) 20 min, (e) 40 min, and (f) 80 min.

To investigate the formation of rod-type  $\text{Cu}_6(\text{Sn},\text{In})_5$  at the interface, the sample after soldering at 150 °C for 80 min was observed with a low magnification SEM image, as shown in Figure 7. In addition to the rod-type  $\text{Cu}_6(\text{Sn},\text{In})_5$  precipitates at the interface, water quenching results in some sporadic rod-type  $\text{Cu}_6(\text{Sn},\text{In})_5$  precipitation in the In-48Sn solder matrix far away from the interface. A precipitate-free zone could be observed above the In-48Sn/Cu interface. These results indicate that rod-type  $\text{Cu}_6(\text{Sn},\text{In})_5$  forms during the cooling process, which is caused by a decrease in Cu solubility in the In-48Sn solder after solidification. During solidification, excess Cu in the In-48Sn solder precipitates. Cu close to the interface is then able to move to the interface and form heterogeneous precipitates when water quenching is applied. On the other hand, Cu that is far from the interface is only able to homogeneously precipitate in situ when quenched with water. However, Cu near the interface is still able to form heterogeneous precipitation. This allows a precipitate-free zone between the heterogeneous precipitation and homogeneous precipitation regions to form.

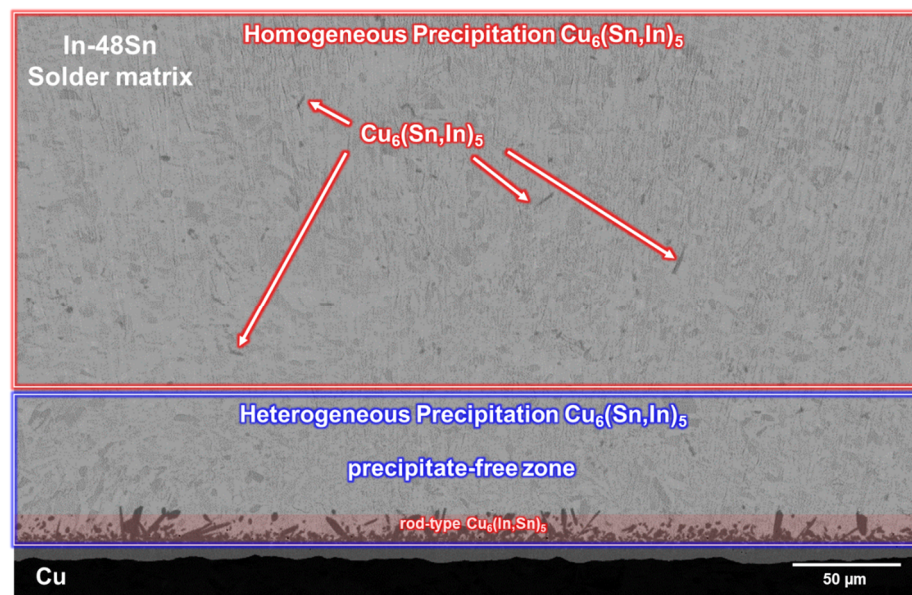


**Figure 7.** Micrograph of the In-48Sn/Cu interface after soldering at 150 °C for 80 min followed by water quenching.

To understand the relationship between Cu concentration and precipitation, the amount of solder was reduced to 0.075 g, while the reaction area was held constant. Just as was performed above, the sample was soldered at 150 °C for 80 min. Figure 8a,b show the top-view morphology, while Figure 8c,d show the interface cross-sections of the two samples prepared with different amounts of solder. According to the cross-sectional microstructure and the position of the  $\text{Cu}_6(\text{Sn,In})_5/\text{Cu}$  interface, the total Cu consumption is consistent between the two samples. This is because the Cu concentration in In-48Sn is well below the saturation concentration, and, therefore, the dissolution rate and amount of  $\text{Cu}_6(\text{Sn,In})_5$  are related to the soldering time rather than Cu concentration. Because Cu dissolved in In-48Sn is equal to Cu consumption, and Cu exists as  $\text{Cu}_6(\text{Sn,In})_5$ , these two samples have the same Cu consumption and amount of  $\text{Cu}_6(\text{Sn,In})_5$ . This indicates that the total Cu in both amounts of In-48Sn solder is the same. The molten In-48Sn solidified as  $\beta$  and  $\gamma$  phases when cooled to room temperature (25 °C). Because Cu is almost completely insoluble in both the  $\beta$  and  $\gamma$  phases, the supersaturated Cu in the solder matrix precipitates in the form of  $\text{Cu}_6(\text{Sn,In})_5$  after cooling. Based on these observations, the Cu concentration in the sample using 0.075 g of solder was twice that of the sample using 0.15 g of solder. This increase in Cu concentration results in denser rod-type  $\text{Cu}_6(\text{Sn,In})_5$  heterogeneous precipitation at the interface (Figure 8d). Conversely, the sample using 0.15 g solder has more homogeneous precipitation in its solder matrix (Figure 8c). Furthermore, the sum of the heterogeneous and homogeneous precipitation remains the same between the two samples.

A previous study reported that discontinuous  $\text{Cu}_6(\text{Sn,In})_5$  around rod-type  $\text{Cu}_6(\text{Sn,In})_5$  was caused by spalling. However, based on the proposed formation mechanism and random growth direction of  $\text{Cu}_6(\text{Sn,In})_5$  from the top view, the discontinuous  $\text{Cu}_6(\text{Sn,In})_5$  was determined to be not due to spalling but rather truncated rod-type  $\text{Cu}_6(\text{Sn,In})_5$ .

A schematic of the proposed mechanism for the interfacial reaction between the liquid In-48Sn and solid Cu at 150 °C is illustrated in Figure 9. At the beginning of soldering, a thin  $\text{Cu}_6(\text{Sn,In})_5$  layer forms at the In-48Sn interface. Then, the  $\text{Cu}_6(\text{Sn,In})_5$  layer continues to grow and is simultaneously dissolved by the molten In-48Sn solder as soldering proceeds. Finally, rod-type  $\text{Cu}_6(\text{Sn,In})_5$  precipitates after cooling due to the difference in Cu solubility between liquid and solid In-48Sn.

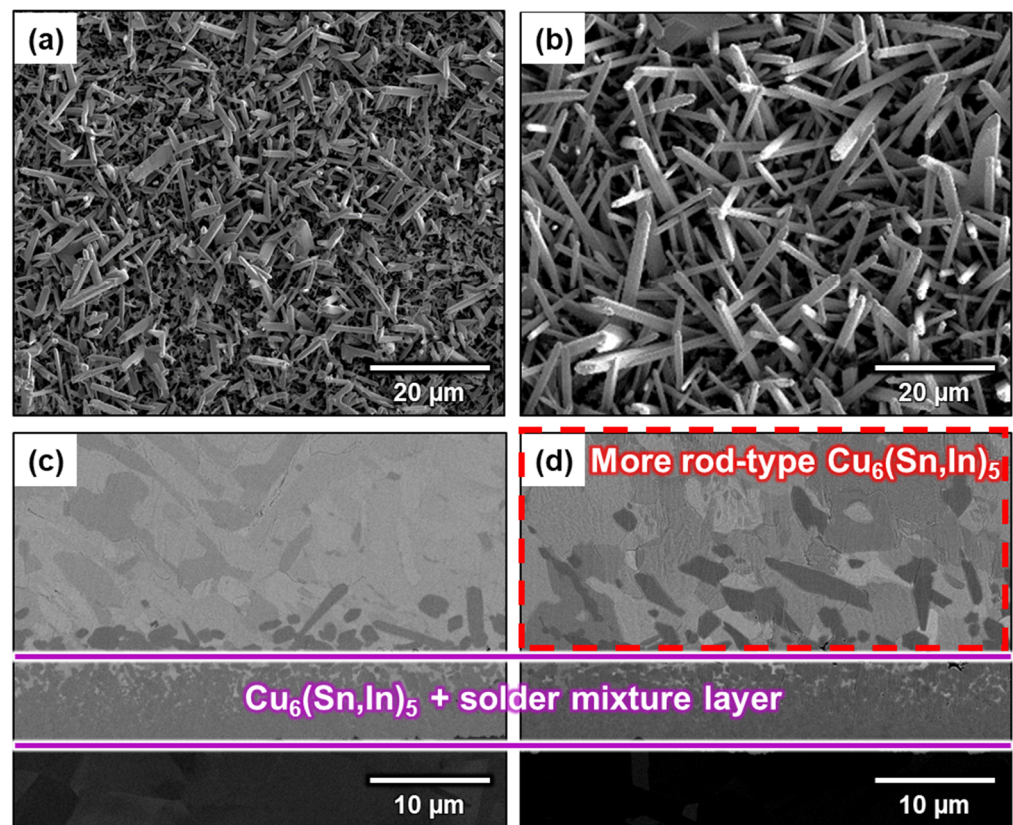


**Figure 8.** Micrographs of the interfaces after soldering at 150 °C for 80 min using different amounts of In-48Sn solder: (a) 0.15 g/top view, (b) 0.075 g/top view, (c) 0.15 g/cross-section, and (d) 0.075 g/cross-section.

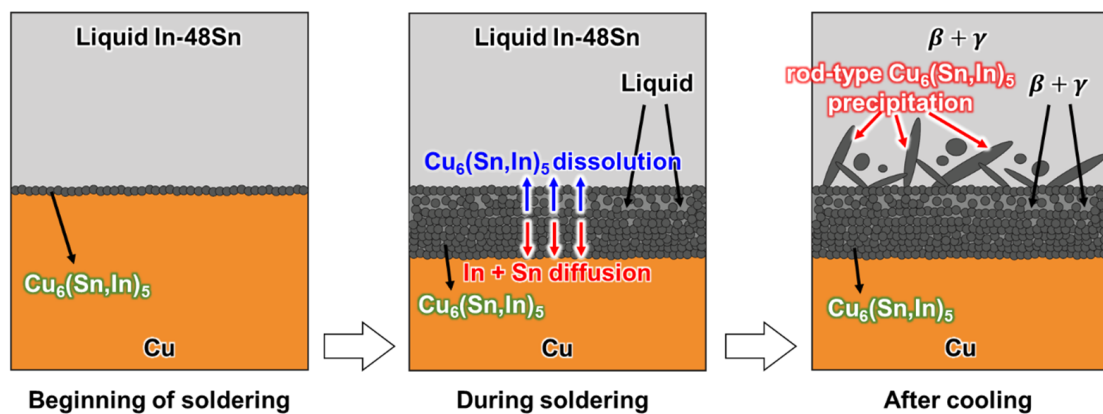


**Figure 9.** Schematic of the microstructure evolution between the liquid In-48Sn and solid Cu at 150 °C soldering.

### 3.4. Room-Temperature Aging

A previous study reported the formation of both  $\text{Cu}_6(\text{Sn,In})_5$  and  $\text{Cu}(\text{In,Sn})_2$  IMCs during soldering at 160 °C. However, the formation of  $\text{Cu}(\text{In,Sn})_2$  at the interface after soldering at 150 °C was not observed in this study. It is possible that  $\text{Cu}(\text{In,Sn})_2$  was not formed during soldering but during room-temperature storage. Because 25 °C is approximately 0.7 times the melting temperature of In, it has been shown to have an apparent creep at room temperature [27,28]. The diffusion of In at room temperature is relatively fast; therefore, interfacial reactions may take place, even at room temperature. To determine the effect of room-temperature storage, the as-bonded samples were stored at room temperature for different amounts of time. The cross-section of the interface after room-temperature storage for 24, 500, and 5000 h is shown in Figure 10a–c. In the sample

aged for 24 h, only the  $\text{Cu}_6(\text{Sn},\text{In})_5$  continuous layer and rod-type  $\text{Cu}_6(\text{Sn},\text{In})_5$  are present at the interface. However, there is no longer rod-type  $\text{Cu}_6(\text{Sn},\text{In})_5$  in the sample stored for 500 h. In contrast, a  $\text{Cu}(\text{In},\text{Sn})_2$  continuous layer formed between the solder matrix and the  $\text{Cu}_6(\text{Sn},\text{In})_5$  layer. After 5000 h of storage at room temperature, the thickness of the  $\text{Cu}(\text{In},\text{Sn})_2$  continuous layer increases, and  $\text{Cu}_6(\text{Sn},\text{In})_5$  becomes a discontinuous layer. This experiment demonstrates that the  $\text{Cu}(\text{In},\text{Sn})_2$  continuous layer formed during room-temperature storage after soldering, which was first reported in the Cu-In-Sn system. This storage process causes unintentional IMC growth under room temperature; hence, this phenomenon is called room-temperature aging.

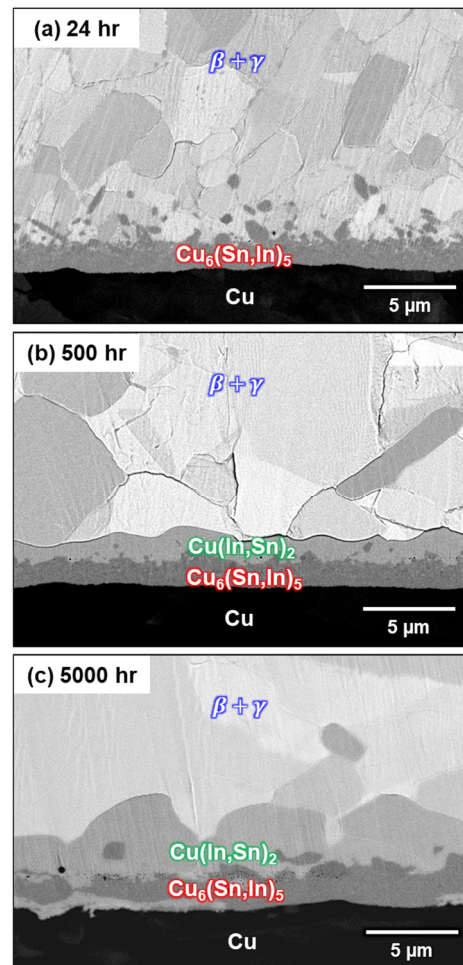


**Figure 10.** Micrographs of the In-48Sn/Cu interfaces after bonding and storage at 25 °C for (a) 24 h, (b) 500 h, and (c) 5000 h.

Phase identification of the  $\text{Cu}(\text{In},\text{Sn})_2$  phase was determined using EPMA and TEM selected area electron diffraction (SAED). The EPMA elemental mapping of the sample aged for 500 h at room temperature is shown in Figure 11. As shown in the EPMA mapping,  $\text{Cu}(\text{In},\text{Sn})_2$  not only exists between the solder and  $\text{Cu}_6(\text{Sn},\text{In})_5$  layer, but all the  $\text{Cu}_6(\text{Sn},\text{In})_5$  precipitated in the solder matrix was transformed into  $\text{Cu}(\text{In},\text{Sn})_2$ . The results of the EPMA quantitative analysis are shown in Table 2. TEM/SAED was used to further confirm the crystal structure of this phase because the thicknesses of these two IMCs are close to the EPMA resolution limit.

Figure 12a shows a TEM bright-field image of both  $\text{Cu}_6(\text{Sn},\text{In})_5$  and  $\text{Cu}(\text{In},\text{Sn})_2$ . The SAED patterns of the  $\text{Cu}(\text{In},\text{Sn})_2$  (b) and  $\text{Cu}_6(\text{Sn},\text{In})_5$  (c) regions are shown in Figure 12b,c, respectively.

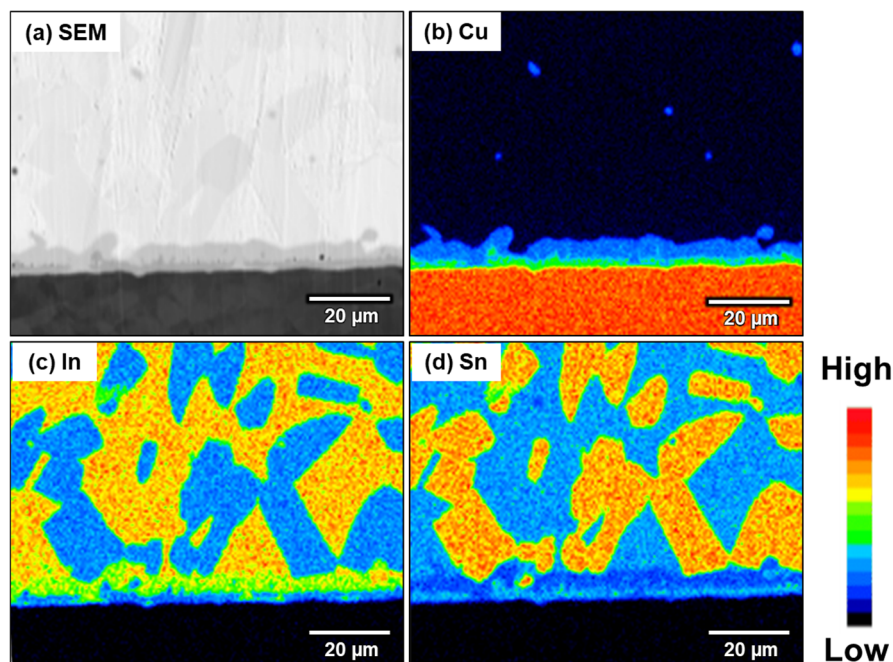


**Figure 11.** EPMA elemental mapping of the In-48Sn/Cu interface after room-temperature aging for 5000 h. (a) SEM, (b) Cu, (c) In, (d) Sn.

**Table 2.** EPMA quantitative analysis of  $\text{Cu}(\text{In},\text{Sn})_2$  and  $\text{Cu}_6(\text{Sn},\text{In})_5$ .

Phase	Cu (at.%)	In (at.%)	Sn (at.%)
$\text{Cu}(\text{In},\text{Sn})_2$	33.4	51.6	15.0
$\text{Cu}_6(\text{Sn},\text{In})_5$	57.3	17.3	25.4

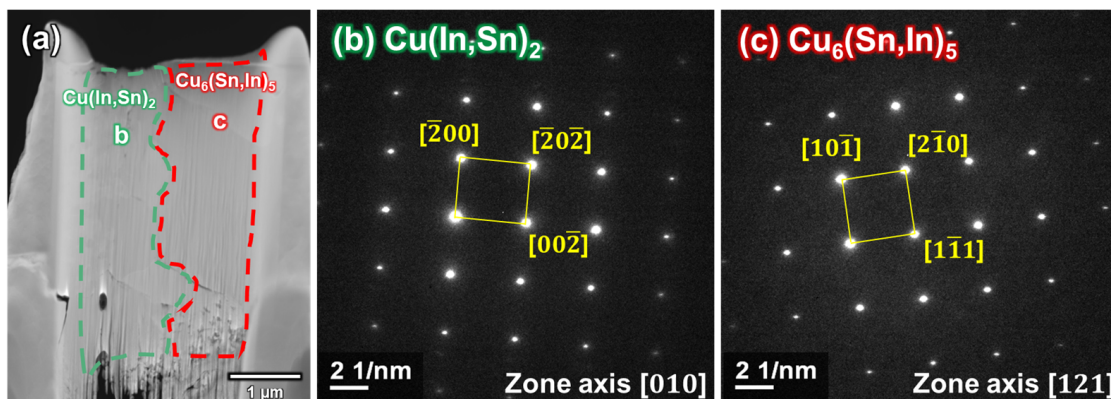


**Figure 12.** TEM imaging of In-48Sn/Cu interface after room temperature aging for 5000 h: (a) TEM bright field image of  $\text{Cu}(\text{In},\text{Sn})_2$  and  $\text{Cu}_6(\text{Sn},\text{In})_5$ , (b) SAED pattern of  $\text{Cu}(\text{In},\text{Sn})_2$ , and (c) SAED pattern of  $\text{Cu}_6(\text{Sn},\text{In})_5$ .

The results of the SAED patterns indicate that the IMC in Figure 12b is  $\text{Cu}(\text{In},\text{Sn})_2$  with a zone axis [010], and the IMC in Figure 12c is  $\text{Cu}_6(\text{Sn},\text{In})_5$  with a zone axis [121]. The crystallographic structure information of  $\eta\text{-Cu}_6\text{Sn}_5$  is from the JCPDS 02-0713, while  $\text{CuIn}_2$  is from the data of Gossila et al. [29].

### 3.5. Mechanical Properties of $\text{Cu}_6(\text{Sn},\text{In})_5$

The mechanical properties of  $\text{Cu}_6\text{Sn}_5$  have been widely studied; however, few studies have investigated the effect of In-doping on the mechanical properties of  $\text{Cu}_6(\text{Sn},\text{In})_5$ .

The mechanical properties of the solder joint and the formed IMCs directly influence the reliability of the bonding results. Here, the effect of adding In on the mechanical properties of  $\text{Cu}_6(\text{Sn},\text{In})_5$  was investigated.

The maximum applied load was 1200  $\mu\text{N}$ , with a 240  $\mu\text{N}/\text{s}$  loading rate, and the maximum load was held for 5 s. The load–displacement curve of  $\text{Cu}_6(\text{Sn},\text{In})_5$  is shown in Figure 13. The Young’s modulus and hardness were averaged from the results of five different points. The measured Young’s modulus and hardness are listed in Table 3 alongside those reported for pure  $\text{Cu}_6\text{Sn}_5$  [30]. As shown in Table 3, both the Young’s modulus and hardness of  $\text{Cu}_6(\text{Sn},\text{In})_5$  are similar to those of pure  $\text{Cu}_6\text{Sn}_5$ .

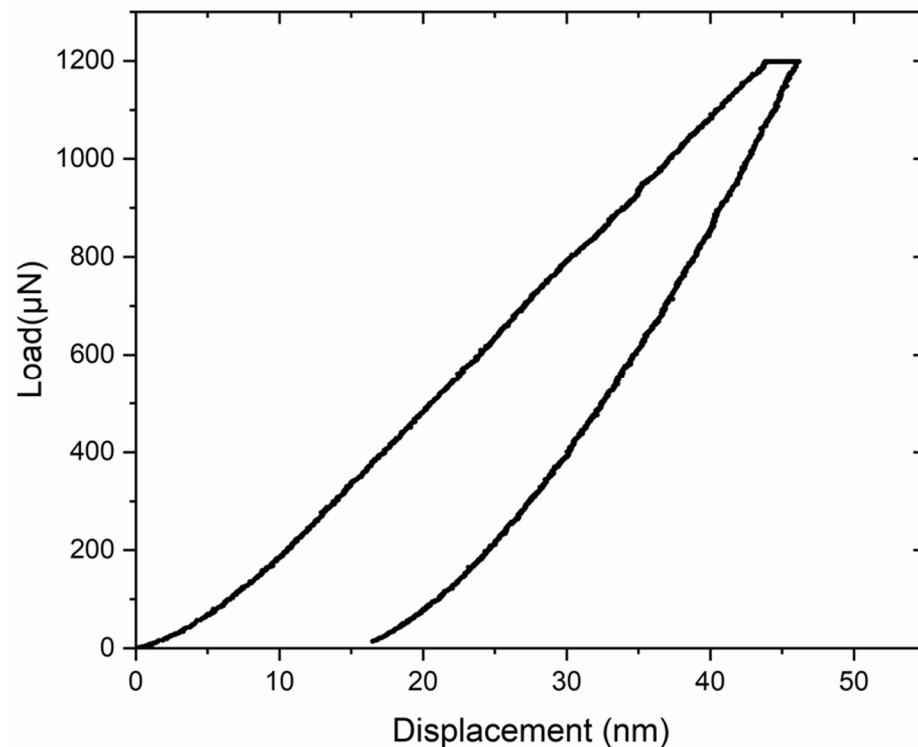


**Figure 13.** Load–displacement curves from the nanoindentation of  $\text{Cu}_6(\text{Sn},\text{In})_5$ .

**Table 3.** Comparison of Young’s modulus and hardness between  $\text{Cu}_6\text{Sn}_5$  and  $\text{Cu}_6(\text{Sn},\text{In})_5$ .

IMC Type	Young’s Modulus (GPa)	Hardness (GPa)
$\text{Cu}_6\text{Sn}_5$ [21]	$118.97 \pm 1.93$	$6.45 \pm 0.14$
$\text{Cu}_6(\text{Sn},\text{In})_5$	$119.04 \pm 3.94$	$6.28 \pm 0.13$

#### 4. Conclusions

In this study, the phase identification, microstructure evolution, and growth mechanism between molten In-48Sn and Cu substrates were investigated. The phase  $\text{Cu}_6(\text{Sn},\text{In})_5$  was identified as the only IMC formed at the interface during soldering at 150 °C, which was confirmed by EPMA quantitative analysis and XRD. A solder/ $\text{Cu}_6(\text{Sn},\text{In})_5$  mixture layer was formed during the soldering process, and the thickness of this layer increased with the soldering time. This layer formed through the simultaneous growth of the  $\text{Cu}_6(\text{Sn},\text{In})_5$  layer and its dissolution by the molten In-48Sn solder. The amount of  $\text{Cu}_6(\text{Sn},\text{In})_5$  in the layer decreases as it approaches the In-48Sn solder. Rod-type  $\text{Cu}_6(\text{Sn},\text{In})_5$  formation was caused by the heterogeneous precipitation of supersaturated Cu in the In-48Sn solder due to a decrease in solubility after solidification.

The formation of  $\text{Cu}(\text{In},\text{Sn})_2$  at the interface was proven to be caused by room-temperature aging after soldering. This result indicates that the In-48Sn/Cu interface cannot be stored at room temperature and needs to be observed immediately after the

experiment; otherwise, room-temperature aging will influence the results of the interfacial reaction. The Young's modulus and hardness of  $\text{Cu}_6(\text{Sn},\text{In})_5$  were determined to be  $119.04 \pm 3.94$  GPa and  $6.28 \pm 0.13$  GPa, respectively, indicating that the addition of In to  $\text{Cu}_6(\text{Sn},\text{In})_5$  did not have a significant impact on Young's modulus and hardness.

In this study, although the formation of  $\text{Cu}(\text{In},\text{Sn})_2$  caused by room-temperature aging was reported, the critical temperature at which  $\text{Cu}(\text{In},\text{Sn})_2$  starts to appear was not determined, so further studies are still needed.

**Author Contributions:** Conceptualization, F.-L.C. and C.-W.K.; Methodology, F.-L.C. and H.-T.H.; Validation, F.-L.C.; Formal analysis, F.-L.C. and Y.-H.L.; Investigation, F.-L.C., Y.-H.L. and C.-W.K.; Resources, C.R.K.; Data curation, F.-L.C.; Writing—original draft, F.-L.C.; Writing—review & editing, H.-T.H. and C.R.K.; Visualization, F.-L.C.; Project administration, C.R.K.; Funding acquisition, C.R.K. All authors have read and agreed to the published version of the manuscript.

**Funding:** This research was funded by the National Science and Technology Council (Taiwan NSTC) through Grant MOST 111-2223-E-002-009.

**Institutional Review Board Statement:** Not applicable.

**Informed Consent Statement:** Not applicable.

**Data Availability Statement:** Not applicable.

**Acknowledgments:** Financial support from the National Science and Technology Council (Taiwan NSTC) through Grant MOST 111-2223-E-002-009 is acknowledged. The authors thank the technical help provided by Ya-Yun Yang and Ching-Yen Lin from the Precious Instrument Center of the College of Science at National Taiwan University for their assistance with the ion milling.

**Conflicts of Interest:** The authors declare no conflict of interest.

## References

1. Zhang, L.; Tu, K.N. Structure and properties of lead-free solders bearing micro and nano particles. *Mater. Sci. Eng. R Rep.* **2014**, *82*, 1–32. [[CrossRef](#)]
2. Kotadia, H.R.; Howes, P.D.; Mannan, S.H. A review: On the development of low melting temperature Pb-free solders. *Microelectron. Reliab.* **2014**, *54*, 1253–1273. [[CrossRef](#)]
3. Gain, A.; Zhang, L. Effect of Ag nanoparticles on microstructure, damping property and hardness of low melting point eutectic tin–bismuth solder. *J. Mater. Sci. Mater. Electron.* **2017**, *28*, 15718–15730. [[CrossRef](#)]
4. Freer, J.; Morris, J. Microstructure and creep of eutectic indium/tin on copper and nickel substrates. *J. Electron. Mater.* **1992**, *21*, 647–652. [[CrossRef](#)]
5. Faizov, S.; Sarafanov, A.; Erdakov, I.; Gromov, D.; Svistun, A.; Glebov, L.; Bykov, V.; Bryk, A.; Radionova, L. On the Direct Extrusion of Solder Wire from 52In-48Sn Alloy. *Machines* **2021**, *9*, 93. [[CrossRef](#)]
6. Tian, F.; Liu, Z.-Q.; Shang, P.-J.; Guo, J. Phase identification on the intermetallic compound formed between eutectic SnIn solder and single crystalline Cu substrate. *J. Alloys Compd.* **2014**, *591*, 351–355. [[CrossRef](#)]
7. Shang, P.; Liu, Z.; Li, D.; Shang, J. Intermetallic compound identification and Kirkendall void formation in eutectic SnIn/Cu solder joint during solid-state aging. *Philos. Mag. Lett.* **2011**, *91*, 410–417. [[CrossRef](#)]
8. Tian, F.-f.; Liu, Z.-q. The interfacial microstructure and Kirkendall voids in In-48Sn/Cu solder joint. In Proceedings of the 2013 14th International Conference on Electronic Packaging Technology, Dalian, China, 11–14 August 2013; pp. 907–910.
9. Susan, D.; Rejent, J.; Hlava, P.; Vianco, P. Very long-term aging of 52In-48Sn (at.%) solder joints on Cu-plated stainless steel substrates. *J. Mater. Sci.* **2009**, *44*, 545–555. [[CrossRef](#)]
10. Liu, Z.-Q.; Tian, F.-F. The reversible transformation between  $\text{Cu}_2(\text{In}, \text{Sn})$  and  $\text{Cu}(\text{In}, \text{Sn})_2$  compounds during solid-state aging. In Proceedings of the 2014 15th International Conference on Electronic Packaging Technology, Chengdu, China, 12–15 August 2014; pp. 425–428.
11. Tian, F.; Liu, Z.-Q. Growth mechanism of duplex structural  $\text{Cu}_2(\text{In}, \text{Sn})$  compound on single crystalline Cu substrate. *J. Alloy. Compd.* **2014**, *588*, 662–667. [[CrossRef](#)]
12. Tian, F.; Liu, Z.-Q.; Guo, J. Phase transformation between  $\text{Cu}(\text{In}, \text{Sn})_2$  and  $\text{Cu}_2(\text{In}, \text{Sn})$  compounds formed on single crystalline Cu substrate during solid state aging. *J. Appl. Phys.* **2014**, *115*, 043520. [[CrossRef](#)]
13. Tian, F.; Shang, P.-J.; Liu, Z.-Q. Precise Cr-marker investigation on the reactive interface in the eutectic SnIn solder joint. *Mater. Lett.* **2014**, *121*, 185–187. [[CrossRef](#)]
14. Li, Y.; Lim, A.B.; Luo, K.; Chen, Z.; Wu, F.; Chan, Y. Phase segregation, interfacial intermetallic growth and electromigration-induced failure in Cu/In-48Sn/Cu solder interconnects under current stressing. *J. Alloy. Compd.* **2016**, *673*, 372–382. [[CrossRef](#)]

15. Tian, F.; Li, C.-F.; Zhou, M.; Liu, Z.-Q. The interfacial reaction between In-48Sn solder and polycrystalline Cu substrate during solid state aging. *J. Alloy. Compd.* **2018**, *740*, 500–509. [[CrossRef](#)]
16. Han, D.L.; Shen, Y.-A.; He, S.; Nishikawa, H. Effect of Cu addition on the microstructure and mechanical properties of In–Sn-based low-temperature alloy. *Mater. Sci. Eng. A* **2021**, *804*, 140785. [[CrossRef](#)]
17. Han, D.L.; Tatsumi, H.; Huo, F.; Nishikawa, H. Effect of isothermal aging on properties of In-48Sn and In-Sn-8Cu alloys. In Proceedings of the 2022 IEEE 72nd Electronic Components and Technology Conference (ECTC), San Diego, CA, USA, 31 May–3 June 2022; pp. 2148–2152.
18. Hotchkiss, J.; Vuorinen, V.; Dong, H.; Ross, G.; Kaaos, J.; Paulasto-Krockel, M.; Wernicke, T.; Ponninger, A. Study of Cu-Sn-In system for low temperature, wafer level solid liquid inter-diffusion bonding. In Proceedings of the 2020 IEEE 8th Electronics System-Integration Technology Conference (ESTC), Tonsberg, Norway, 15–18 September 2020; pp. 1–5.
19. Song, R.-W.; Fleshman, C.J.; Chen, H.; Tsai, S.-Y.; Duh, J.-G. Suppressing interfacial voids in Cu/In/Cu microbump with Sn and Cu addition. *Mater. Lett.* **2020**, *259*, 126855. [[CrossRef](#)]
20. Vuorinen, V.; Ross, G.; Klami, A.; Dong, H.; Paulasto-Krockel, M.; Wernicke, T.; Ponninger, A. Demonstrating 170°C Low Temperature Cu-In-Sn wafer level Solid Liquid Interdiffusion Bonding. *IEEE Trans. Compon. Packag. Manuf. Technol.* **2021**, *12*, 446–453. [[CrossRef](#)]
21. Han, D.L.; Shen, Y.-A.; Huo, F.; Nishikawa, H. Microstructure Evolution and Shear Strength of Tin-Indium-xCu/Cu Joints. *Metals* **2022**, *12*, 33. [[CrossRef](#)]
22. Kang, D.G.; Min, K.D.; Jung, H.S.; Ha, E.; Kim, K.Y.; Jung, S.B. Mechanical properties and microstructures of Cu/In-48Sn alloy/Cu with low temperature TLP bonding. In Proceedings of the 2022 IEEE 72nd Electronic Components and Technology Conference (ECTC), San Diego, CA, USA, 31 May–3 June 2022; pp. 2206–2210.
23. Vianco, P.T.; Hlava, P.F.; Kilgo, A.C. Intermetallic compound layer formation between copper and hot-dipped 100In, 50In-50Sn, 100Sn, and 63Sn-37Pb coatings. *J. Electron. Mater.* **1994**, *23*, 583–594. [[CrossRef](#)]
24. Hung, H.; Lee, P.; Tsai, C.; Kao, C. Artifact-free microstructures of the Cu–In reaction by using cryogenic broad argon beam ion polishing. *J. Mater. Res. Technol.* **2020**, *9*, 12946–12954. [[CrossRef](#)]
25. Shu, Y.; Ando, T.; Yin, Q.; Zhou, G.; Gu, Z. Phase diagram and structural evolution of tin/indium (Sn/In) nanosolder particles: From a non-equilibrium state to an equilibrium state. *Nanoscale* **2017**, *9*, 12398–12408. [[CrossRef](#)]
26. Zeng, G.; McDonald, S.D.; Gu, Q.; Nogita, K. Effect of Zn, Au, and In on the polymorphic phase transformation in Cu<sub>6</sub>Sn<sub>5</sub> intermetallics. *J. Mater. Res.* **2012**, *27*, 2609–2614. [[CrossRef](#)]
27. Feng, G.; Ngan, A. Creep and strain burst in indium and aluminium during nanoindentation. *Scr. Mater.* **2001**, *45*, 971–976. [[CrossRef](#)]
28. Lucas, B.; Oliver, W. Indentation power-law creep of high-purity indium. *Metall. Mater. Trans. A* **1999**, *30*, 601–610. [[CrossRef](#)]
29. Gossila, M.; Metzner, H.; Mahnke, H.E. Coevaporated Cu–In films as precursors for solar cells. *J. Appl. Phys.* **1999**, *86*, 3624–3632. [[CrossRef](#)]
30. Yang, P.-F.; Lai, Y.-S.; Jian, S.-R.; Chen, J.; Chen, R.-S. Nanoindentation identifications of mechanical properties of Cu<sub>6</sub>Sn<sub>5</sub>, Cu<sub>3</sub>Sn, and Ni<sub>3</sub>Sn<sub>4</sub> intermetallic compounds derived by diffusion couples. *Mater. Sci. Eng. A* **2008**, *485*, 305–310. [[CrossRef](#)]

**Disclaimer/Publisher’s Note:** The statements, opinions and data contained in all publications are solely those of the individual author(s) and contributor(s) and not of MDPI and/or the editor(s). MDPI and/or the editor(s) disclaim responsibility for any injury to people or property resulting from any ideas, methods, instructions or products referred to in the content.